AIAA JOURNAL
Vol. 36, No. 10, October 1998

Time-Series Analyses of Wall Pressure Fluctuations in Plume-Induced Separated Flowfields

R. J. Shaw*
SY Technology, Inc., Huntsville, Alabama 35806
and
J. C. Dutton† and A. L. Addy‡
University of Illinois at Urbana–Champaign, Urbana, Illinois 61801

The separation shock wave motion in a plume-induced, boundary-layer separated flowfield was studied experimentally. The statistical properties of the shock wave motion were determined over the intermittent region using time-series analyses of wall static pressure fluctuation measurements. The standard deviation of the pressure fluctuations, nondimensionalized by the local mean pressure, reached a maximum of 0.22 near the middle of the intermittent region. The ratio of the maximum standard deviation of the pressure fluctuations over the intermittent region to the mean pressure difference across the intermittent region was calculated to be 0.43 for this flowfield. Both of these quantities demonstrate that the unsteady pressure loading caused by the shock wave motion has essentially the same magnitude in plume-induced separated flowfields as in flowfields produced by solid boundary protuberances.

Introduction

THE phenomenon of plume-induced boundary-layer separation (PIBLS) occurs on atmospheric flight vehicles when the boundary layer on the afterbody separates upstream of the base, rather than at the base, as a result of the exhaust plume expanding into and interacting with the external freestream. The unsteady separation shock wave motion, which is known to accompany the occurrence of plume-induced, turbulent boundary-layer separation,[1] is a topic that has received little attention in the past and is the subject of the present investigation.

The only studies of unsteady shock wave motion associated with plume-induced separation known to the authors were conducted with a wall-mounted, cone-cylinder-finned model in a variable Mach number (2.5–3.5) wind tunnel.[2–4] A secondary jet of cold air, at an exit plane Mach number of 2.94 and an angle of 74 deg with respect to the freestream flow direction, exhausted from a conical nozzle near the aft end of the model. The capability of pulsing the plume was included in the wind-tunnel model design to simulate combustion instabilities of liquid propellant engines. In summary, these studies found a natural unsteadiness associated with the separation process in all of the PIBLS flowfields produced with the wind-tunnel model (even in the absence of plume pulsing).[2–4] Based on measurements made from numerous schlieren movie frames, the unsteadiness associated with the separation process produced a length scale for the intermittent region that was on the order of a few boundary-layer thicknesses. A sparsely distributed set of fast-response pressure transducer measurements was made across the intermittent region, i.e., the region of shock wave motion, and analyzed using standard time-series analysis techniques. A power spectral density estimate computed from one of the pressure-time histories suggested that the energy of the pressure fluctuations associated with the shock wave motion had a dominant characteristic frequency of approximately 100 Hz and was mostly contained below 1 kHz. The effect on the separation shock wave motion of pulsing the plume flow at discrete frequencies over the range between 12.5 Hz and 1 kHz was minimal. Rather than the separation shock wave oscillating at the discrete pulsing frequency of the plume, the separation shock wave motions occurred over a wide frequency range regardless of the plume pulsing frequency.

In contrast to the unsteadiness found in shock wave/turbulent boundary-layer interactions (SWBLIs) caused by a compliant aerodynamic boundary (PIBLS flowfields), unsteadiness in SWBLI flowfields produced by solid boundary protuberances has received a significant amount of attention over the past 15 years.[5] Pressure fluctuation measurements have been made over the intermittent regions of SWBLI flowfields produced by compression ramps,[6–8] effectively semi-infinite circular cylinders,[9,10] sharp-edged fins at angles of attack,[11,12] and hemicylindrical blunt-edged fins at angles of attack.[13,14] The unsteady characteristics of the shock wave motion have been determined for these geometries by analyzing both individually and simultaneously acquired pressure-time histories with standard time-series analysis techniques and conditional analysis methods. Although quantitative differences in the unsteady characteristics of the separation shock wave motion exist for these four geometries, the characteristics found in these interactions qualitatively show many similar features. The similarities include bimodal probability density function (PDF) estimates of the pressure fluctuation amplitudes over the intermittent region, streamwise distributions of the standard deviation of the pressure fluctuations that reach rather large (relative to the incoming boundary layer and the separated flowfield) maximum values near the middle of the intermittent region, and streamwise distributions of the skewness and kurtosis coefficients that reach rather large values near the upstream edge of the intermittent region. Also, in nominally two-dimensional or quasi-two-dimensional interactions, the power spectral density (PSD) estimates show that most of the energy contained in the pressure fluctuations caused by the shock wave motion is distributed over the frequency range between approximately 100 Hz and 1 kHz. The range of frequencies associated with the energy contained in the pressure fluctuations caused by the shock wave motion increases as the sweepback angle of the interaction increases for the compression ramp, circular cylinder, and blunt- and sharp-edged fin geometries.[15]

A two-part model that describes the physical mechanisms responsible for the unsteady separation shock wave motion in SWBLI flowfields has recently been hypothesized.[16] The model divides the separation shock wave motions into small-scale or jittery motions and large-scale or global motions. In the first part, the shock wave motions are caused by fluctuations (attributed to turbulence in the incoming boundary layer near the separation shock) in the ratio of static quantities across the shock foot. In the second part, the

Received Sept. 16, 1997; revision received June 23, 1998; accepted for publication June 25, 1998.

*Research Engineer.
†W. Grafton and Lillian B. Wilkins Professor, Department of Mechanical and Industrial Engineering. Associate Fellow AIAA.
‡Professor Emeritus, Department of Mechanical and Industrial Engineering. Associate Fellow AIAA.

shock wave motions are caused by the expansions and contractions or "trembling motions" of the separated flow region. Thus, because the internal structure and dynamics of the separation bubble are unique to each type of geometry causing the SWBLI, it is not surprising that each geometry would have a set of unsteady shock wave characteristics with unique quantitative values.

As a result of these experimental studies,[6–15] the statistical characteristics of the separation shock wave motion in SWBLIs produced by solid boundary protuberances have been well documented. These studies have shown that the unsteady separation shock wave motion is responsible for some of the largest aerodynamic loads[17] and highest heat transfer rates[18] that occur in high-speed flight. If the pressure fluctuations in PIBLS flows are similarly large, then the occurrence of PIBLS is indeed important because of the large aerodynamic loads and high heat transfer rates that would undoubtedly accompany the unsteady shock wave motion. However, no experimental measurements of these phenomena exist. Therefore, the objective of the current paper is to determine the unsteady characteristics of the separation shock wave motion in a PIBLS flowfield by analyzing surface pressure fluctuation measurements using standard time-series analysis techniques.

Experimental Program

Wind-Tunnel Facility

The experiments were conducted in the Gas Dynamics Laboratory of the University of Illinois at Urbana–Champaign. A blowdown wind-tunnel facility, which was specifically designed to produce plume-induced separated flowfields, was constructed for this investigation and is shown in Fig. 1. Clean, dry, high-pressure air was supplied to the plenum chamber from a 146-m^3 capacity tank farm and two air compressors, while maintaining a constant stagnation pressure in the plenum chamber with an electropneumatic control valve installed in the air supply line. The plenum chamber fed two inlet pipes that, in turn, fed the two streams of the PIBLS wind-tunnel test section.

A cross-sectional view along the centerline of the PIBLS wind-tunnel test section is shown in the insert of Fig. 1. The test section incorporates a two-dimensional planar geometry and produces two coflowing, uniform, supersonic streams using fixed, converging-diverging, half-nozzles. A flowfield width of 50.8 mm was maintained in the test section from upstream of the nozzle blocks to downstream of the subsonic diffuser. A flow conditioning module, consisting of a honeycomb section and two screens, was installed upstream of each nozzle block. The Mach 1.5 lower stream (inner jet)

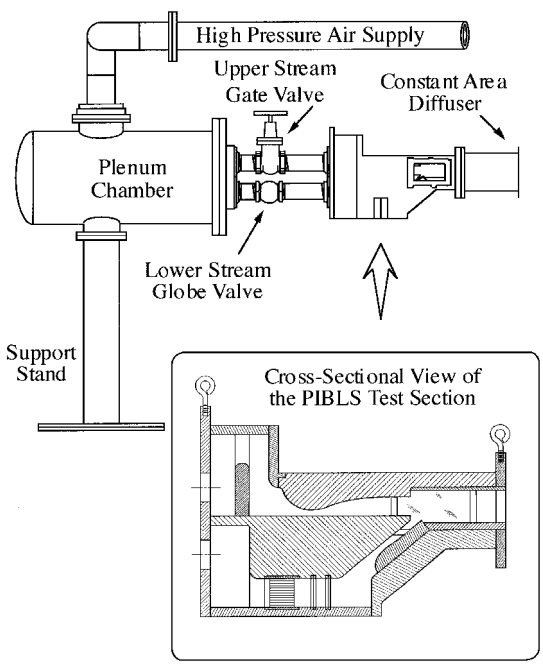

Fig. 1 Schematic of the PIBLS wind-tunnel facility, including an enlarged cross-sectional view of the PIBLS test section.

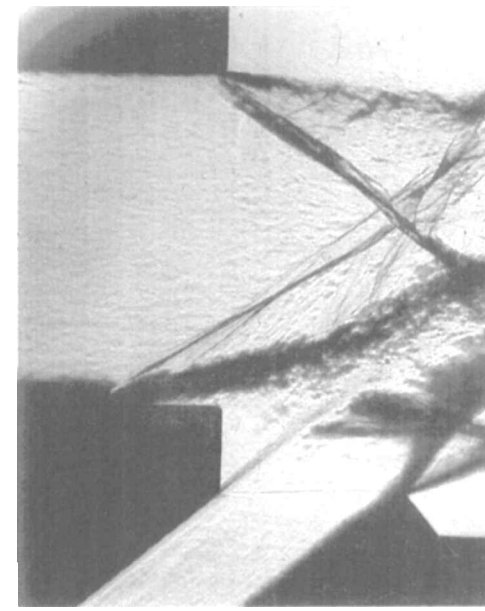

Fig. 2 Schlieren photograph (flashlamp pulse duration of 1.4 μs) of the near-wake region in the PIBLS wind tunnel at a JSPR of approximately 2.35.

impinged upon the Mach 2.5 upper stream (freestream) at a relative angle of 40 deg and across a 12.7-mm base height. Each test section inlet pipe contained a manually adjustable valve for independently regulating the stagnation pressure of each stream. By adjusting the inner jet flow stagnation pressure, the boundary layer on the bottom wall of the freestream was induced to separate upstream of the base corner and thereby form a plume-induced separated flowfield in the test section. A glass window assembly mounted in each sidewall near the base region permitted optical access to the PIBLS flowfield, which was visualized using schlieren and shadowgraph techniques. The schlieren photograph shown in Fig. 2 clearly demonstrates that plume-induced, boundary-layer separation occurs in the test section at a jet-static-pressure-to-freestream-static-pressure ratio (JSPR) of 2.35. When the schlieren (or shadowgraph) light source was operated in the continuous mode, the separation shock wave was clearly seen to undergo streamwise translations at all JSPRs of tunnel operation.

Flow Conditions

The stagnation pressure of each stream was measured with a stagnation pressure probe mounted upstream of each nozzle block, and the stagnation temperature was measured with an iron-constantan thermocouple mounted in the plenum chamber. The data reduction assumed adiabatic flow conditions. The stagnation temperature was 298 K ($\pm$1.5 K). In the freestream, the stagnation pressure was 503 kPa ($\pm$1.5 kPa) and the unit Reynolds number was 47.1×10^6 m^{-1} ($\pm 0.5 \times 10^6$ m^{-1}). The Mach number in this freestream was computed from static pressure measurements made using pressure taps mounted in the lower wall and was found to be 2.50 ($\pm$0.01) at a location 30 mm upstream of the base plane. Similarly, the Mach number of the inner jet was computed to be 1.51 ($\pm$0.01) at a location 12.7 mm upstream of the base plane.

One-component laser Doppler velocimeter (LDV) measurements were made along a vertical centerline traverse across the height of the freestream flow 30 mm upstream of the base plane. From these LDV measurements, the streamwise turbulence intensity was found to be $0.015 \pm 10\%$ across the uniform flow region of the freestream. From the mean velocity measurements made in the boundary layer adjacent to the lower wall of the freestream, a wall-wake velocity profile was curve fitted to the experimental velocity data using the method of Sun and Childs.[19] The details of the procedure are given in Ref. 20. The incoming turbulent boundary-layer properties were determined from the Sun and Childs curve fit and are reported in Table 1. The boundary-layer properties given in Table 1 generally compare favorably with other equilibrium turbulent boundary-layer

Table 1 Incoming turbulent boundary-layer properties in the upper stream

Property	Value
Boundary-layer thickness δ, mm	3.1
Boundary-layer displacement thickness δ^*, mm	0.91
Boundary-layer momentum thickness θ, mm	0.25
Boundary-layer shape factor, $H = \delta^*/\theta$	3.71
Wake strength parameter Π	1.58
Skin-friction coefficient C_f	0.00131
Friction velocity u_τ, m/s	20.6

properties reported in the literature for similar Mach number and Reynolds number conditions.[20] Although the wake strength parameter may be a bit high, Fernholz and Finley[21] suggest that a universal value of Π applicable to all equilibrium turbulent boundary layers may not exist for compressible flows due to upstream history effects.

Instrumentation

Instantaneous wall-pressure fluctuations were measured using two piezoresistive pressure transducers that were flush mounted and spanwise centered in the lower wall of the freestream. The upstream and downstream pressure transducers were located 19.1 and 16.5 mm upstream of the base plane, respectively. The pressure transducers were Kulite Model XCS-062-15G transducers, which had an input pressure range of 103.4 kPa and a nominal full-scale output of 200 mV. Each transducer was configured to operate in the gauge mode; i.e., the transducer produced an output voltage proportional to the pressure difference across the diaphragm. The back side of the diaphragm was referenced to the static pressure of the freestream. Each transducer diaphragm had an active diameter of 0.71 mm; the diaphragm natural frequencies were measured to be 168 and 198 kHz for the upstream and downstream transducers, respectively.[20] The transducers were statically calibrated because shock tube experiments[22] with similar transducers have shown that statically calibrated transducer responses are within a few percent of dynamically calibrated transducer responses. The calibration was performed in situ with a Sensotec Model AG-300 digital pressure gauge equipped with a 206.8-kPa pressure transducer accurate to within ± 103.4 Pa.

The analog output signal from each pressure transducer was amplified with a Measurements Group Model 2311 signal conditioning amplifier and then low-pass filtered using an in-house-built, active Butterworth filter circuit. The amplifier also supplied the 15-V dc excitation source and the appropriate dc offset voltage to the transducer bridge. The amplifier had a continuously variable output voltage gain, which ranged between 25 and 30 for all of the intermittent region measurements, and a -3 dB cutoff frequency of 125 kHz on the wide-band output filter setting (used in all of the experiments described herein). The three-stage, six-pole, in-house-built filter had a fixed voltage gain of 4.3, a -3 dB cutoff frequency of 50 kHz, and an attenuation of -36 dB/octave in the transition band. The output signal from the low-pass filter was digitized with a National Instruments Model NB-A2000 analog-to-digital (A/D) converter installed in an Apple Macintosh IIfx computer. Each channel of the A/D converter was equipped with track-and-hold circuitry and had an input voltage range of ± 5 V and 12-bit resolution. Before every calibration, the voltage gain and dc offset voltage settings on each amplifier were adjusted to maximize the signal-to-noise ratio of the output signal. For the intermittent region measurements, this procedure was done at the largest JSPR used in each set of experiments. The rms signal-to-noise ratios for the pressure fluctuation measurements varied from 15 to 20 in the incoming boundary layer and from 55 to 300 over the intermittent region.

In addition to the two Kulite pressure transducers, 29 static pressure taps were installed in the lower wall adjacent to the freestream. The static pressure ports were 0.64 mm in diameter and were normal to the local surface along a single spanwise plane offset 4.78 mm from the centerline. Twenty-three static pressure ports were uniformly spaced every 1.6 mm beginning at 3.18 mm upstream of the base plane and extending to 38.1 mm upstream of the base plane. The remaining six static pressure ports were uniformly spaced every 6.35 mm starting at 42.9 mm upstream of the base plane. The mean pressure at each static pressure port was measured with a Pressure Systems Model DPT-6400T digital pressure transmitter and stored on a Gateway 2000 486-33 computer. Each static pressure tap was connected to a 0–103.4-kPa pressure transducer mounted in the DPT-6400T using a piece of flexible vinyl tubing approximately 1.5 m long. Also, the stagnation pressure probe used to sense the stagnation pressure in each stream was connected, in the same manner, to a 0–689.5-kPa pressure transducer mounted in the DPT-6400T instrument. The pressure transducers in the DPT-6400T were calibrated with a Consolidated Electrodynamics Type 6-201-0001 dead-weight tester.

Data Acquisition

The two Kulite pressure transducers were rigidly mounted in the test section of the PIBLS wind tunnel. With the pressure transducer locations fixed, the JSPR was varied to move the intermittent region over the transducers. In these experiments, the JSPR was varied by unthrottling the stagnation pressure of the inner jet from 210 to 269 kPa in increments of roughly 3.4 kPa.

Instantaneous wall-pressure fluctuation measurements were made throughout the intermittent region by sampling the two pressure transducers. At each JSPR, the individually sampled pressure transducer measurements were made by sampling the upstream transducer for 24 s at a rate of 166,667 samples/s and then sampling the downstream transducer for 24 s at the same rate. Mean static pressure measurements from the pressure taps in the lower wall of the freestream were also made in conjunction with the individually sampled pressure transducer measurements.

Analysis Techniques

All statistical quantities presented herein were computed using the time-series analysis techniques recommended by Bendat and Piersol.[23] In addition, a conditional analysis method, the two-threshold method box-car conversion (TTMBCC) algorithm,[24] was employed to determine the intermittency (the percentage of time the shock wave was upstream of a given pressure transducer). Before we discuss the results from either the remote (DPT-6400T) or in situ (Kulite) pressure measurements, several comments about the TTMBCC algorithm are appropriate.

The TTMBCC algorithm was developed by Brusniak,[24] Dolling and Brusniak,[25] and Erengil and Dolling[26] at the University of Texas at Austin. As the name suggests, the algorithm employs two threshold levels, $Th_1 = \bar{p}_{wo} + 3\sigma_{p_{wo}}$ and $Th_2 = \bar{p}_{wo} + 6\sigma_{p_{wo}}$, where $\bar{p}_{wo}$ is the mean pressure of the incoming boundary layer and $\sigma_{p_{wo}}$ is the rms of the pressure fluctuations in the incoming boundary layer. By comparing each individual pressure realization in a pressure-time history to the two threshold levels, the instantaneous location of the separation shock wave can be determined as being either upstream or downstream of the pressure transducer. The precise time (to within the sampling period) when the shock wave crosses upstream of the pressure transducer, called the rise time, and downstream of the pressure transducer, called the fall time, can be determined for all shock wave passages in the pressure-time history. The intermittency is then calculated from

$$\gamma = \frac{\sum_{k=1}^{N_{sc}} (\mathrm{Fall}_k - \mathrm{Rise}_k)}{\mathrm{Fall}_{N_{sc}} - \mathrm{Rise}_1} \tag{1}$$

where Fall_k is the fall time associated with the kth downstream shock wave crossing, Rise_k is the rise time associated with the kth upstream shock wave crossing, and N_{sc} is the total number of fall times detected in the pressure-time history.

The intermittency calculations performed in the current study used, without any significant changes, the updated version of the TTMBCC algorithm.[26] A sensitivity analysis of the TTMBCC algorithm was performed with the PIBLS data[20] to evaluate the change in magnitude of the zero-crossing frequency, i.e., the average number of shock wave crossings per second, to different threshold level settings. After comparing the results from the sensitivity analysis performed on the PIBLS data to the results from the sensitivity analysis performed on Mach 5 circular cylinder interaction data,[25] it was concluded that the optimal settings for Th_1 and Th_2 given earlier

were also reasonable choices for conditionally analyzing the data from the PIBLS flowfield experiments.[20]

We also note that, by normalizing the rms of the pressure fluctuations in the incoming boundary layer with respect to the wall shear stress and freestream dynamic pressure, the values $\sigma_{p_{wo}}/\tau_w = 3.30$ and $\sigma_{p_{wo}}/q_\infty = 0.0044$ are obtained. These are consistent with previous studies of supersonic turbulent boundary layers.[20]

Results

Results from the remote and in situ pressure transducer measurements will be presented and discussed in the following sections. Although the lower stream stagnation pressure, or the JSPR, was the actual independent variable in the experiments, some of the results will be presented as a function of intermittency rather than JSPR. A plot of intermittency vs JSPR over the intermittent region is shown in Fig. 3 for both the upstream and downstream individually sampled transducer measurements. Whereas the downstream transducer measurements spanned the intermittent region from $\gamma = 3.9$ to 96.2% over a range of JSPR from 1.95 to 2.41, the upstream transducer measurements spanned the intermittent region from $\gamma = 3.8$ to 98.3% over a range of JSPR from 2.05 to 2.49.

Mean Pressure Measurements

At each JSPR shown in Fig. 3, four mean pressure data sets were acquired with the DPT-6400T transmitter under identical wind-tunnel operating conditions. The four data sets were then averaged, and the result is reported as the mean pressure distribution along the lower wall of the freestream. Figure 4 shows the mean static pressure distribution at five strategic JSPRs. Each distribution is plotted in terms of absolute pressure vs distance from the base plane X. The X axis is assumed to be positive in the downstream direction, and $X = 0$ is at the base plane. Each of the mean static pressure distributions is labeled with the appropriate JSPR and the intermittency computed from the downstream pressure transducer measurements. Also, the mean pressures determined from the upstream and downstream in situ pressure transducer measurements (labeled as Kulites) are shown in Fig. 4.

In addition to spanning the intermittent region, each of the streamwise mean static pressure distributions shown in Fig. 4 includes part of the incoming boundary layer and part of the separated flowfield downstream of the intermittent region. All of the distributions show that the mean pressure level of the incoming turbulent boundary layer is constant at approximately 29.6 kPa over the JSPR range from 1.95 to 2.41. The location where the mean static pressure first rises above the mean pressure level of the incoming turbulent boundary layer, called the line of upstream influence, moved farther upstream of the base plane as the JSPR increased from 1.95 to 2.41, as expected. The mean static pressure level in the separated flowfield was not constant over this JSPR range, nor was the mean static pressure distribution over the separated flowfield constant at any JSPR. Fully separated flow existed immediately downstream of the downstream pressure transducer location at a JSPR of 2.41; the mean pressure distribution for this case shows that a significant adverse pressure gradient existed in the separated flowfield. Based on the other mean static pressure distributions shown in Fig. 4, a significant adverse mean pressure gradient existed in the separated flowfield at other JSPR settings as well.

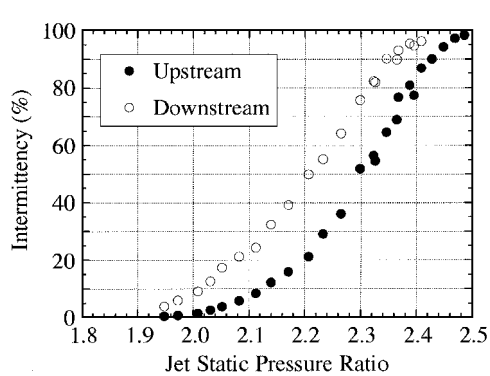

Fig. 3 Plot of intermittency vs JSPR for the upstream and downstream pressure transducer measurements.

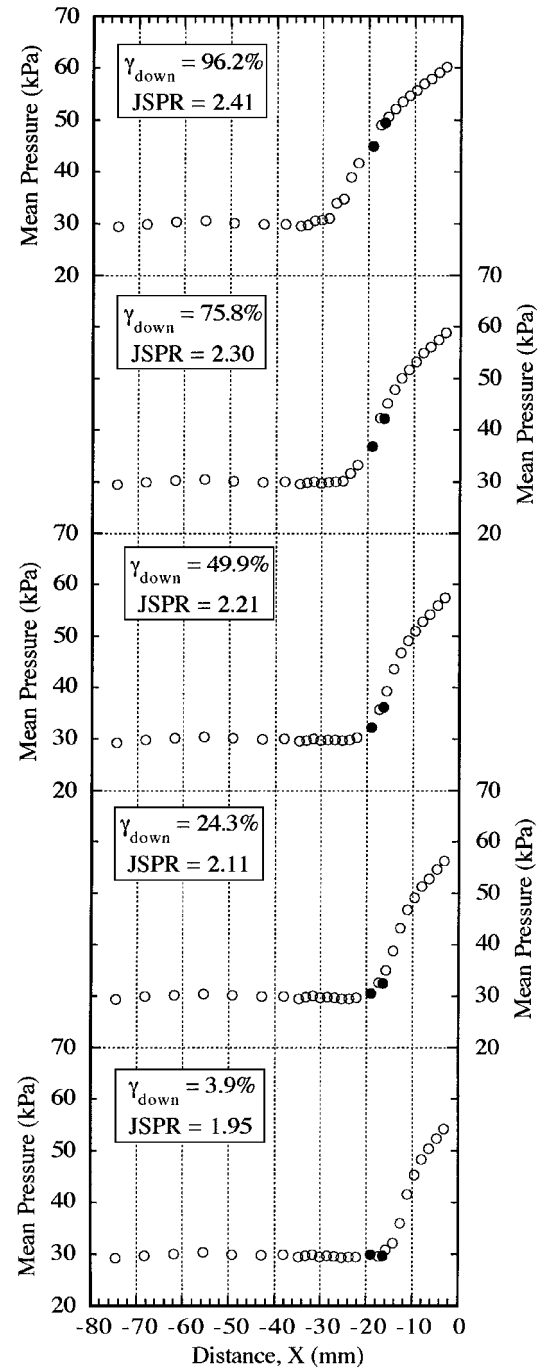

Fig. 4 Mean static pressure distributions on the lower wall of the freestream at five JSPRs (●, Kulites, and ○, DPT-6400T).

The mean pressure measured with the two in situ pressure transducers was observed to be slightly lower than the mean pressure measured with the static pressure taps over most of the intermittent region. This discrepancy is a well-known problem[27] in wind-tunnel experiments involving unsteady pressure fields and exists because of pneumatic resonance effects that occur within the large length/diameter tubing connecting the remote pressure transducers to the static pressure taps. The mean pressures computed from the static taps were, at worst, no more than 10% larger than the mean pressures calculated from the in situ pressure transducers over the intermittent region. Because the mean pressure from the static pressure tap measurements was within approximately 1% of the mean pressure determined from the in situ pressure transducer measurements in both the low ($\gamma < 5\%$) and high ($\gamma > 95\%$) intermittency ranges, the mean pressure can be determined from the static pressure

tap measurements near the line of upstream influence and near the separation line. This fact, when combined with the fast-response pressure transducer measurements and oil-streak visualization images, was used to estimate the length of the intermittent region.[20] With the intermittent region defined to exist between the $\gamma = 4$ and 96% locations for any JSPR, the length of the intermittent region was estimated as 8.1–9.4 mm ($2.6\delta_o$–$3.0\delta_o$) and 17.3–17.5 mm ($5.4\delta_o$–$5.5\delta_o$) at JSPRs of 1.95 and 2.41, respectively. Thus, as the JSPR increased from 1.95 to 2.41, not only did the intermittent region become longer, but also the separated flow region became longer and, in so doing, pushed the intermittent region farther upstream.

PDF Estimates of the Pressure Fluctuation Amplitudes

PDF estimates of the pressure fluctuation amplitudes were calculated at each JSPR for the upstream and downstream pressure transducer measurements. The trends in the PDF estimates over the intermittent region were similar for the upstream and downstream transducer data. Figure 5 shows PDF estimates of the pressure fluctuation amplitudes calculated from the downstream pressure transducer measurements in the incoming turbulent boundary layer, across the intermittent region at the same five JSPRs as Fig. 4, and in the fully separated region at a JSPR of 2.52. Each of the PDF estimates is plotted in terms of $N_i/(N_t \times W)$ vs pressure, where N_i is the number of pressure realizations occurring with a value of $p_i \pm W/2$, N_t is the total number of pressure realizations in the pressure-time history, and W is the interval width of the PDF estimate centered at p_i ($W = 172$ Pa). Also shown in Fig. 5 is the equivalent Gaussian PDF (with the same mean and standard deviation as the actual PDF) for each of the seven estimates.

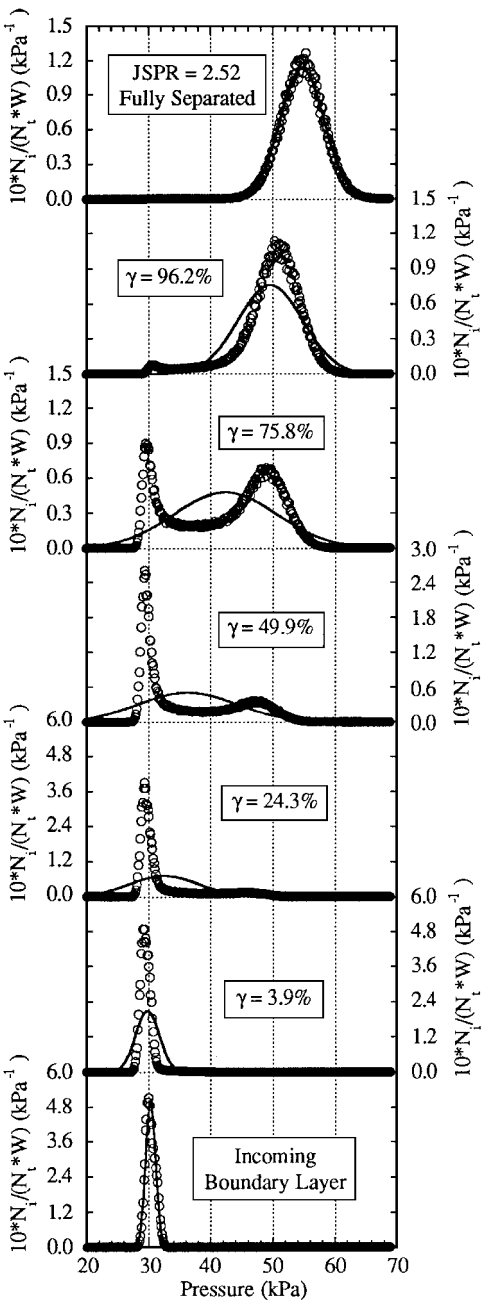

Fig. 5 PDF estimates of the pressure fluctuation amplitudes across the intermittent region (○, actual PDF, and ——, Gaussian PDF). JSPR values identical to those in Fig. 4 at the same γ.

The actual PDFs were essentially Gaussian distributions in the incoming boundary layer and in the fully separated region downstream of the intermittent region. The width of the PDF was much larger for the fully separated region at a JSPR of 2.52 than for the incoming boundary layer, indicating that the pressure fluctuation amplitudes were larger in the fully separated region than in the boundary layer.

The actual PDF was strongly skewed from its equivalent Gaussian distribution at each JSPR over the intermittent region. At low intermittency values ($\gamma < 25\%$), only a single visible peak was present in the actual PDF, and the maximum probability associated with this peak occurred at approximately 29.6 kPa. The cause of the peak was clearly the pressure fluctuations present in the incoming turbulent boundary layer. Although not enough pressure fluctuations from the separated flowfield downstream of the shock wave were present to visibly skew the actual PDF into a bimodal shape at these JSPRs, the equivalent Gaussian PDF was widened noticeably beyond the width of the actual PDF peak caused by the incoming turbulent boundary layer. This was because the pressure fluctuations that were present from the separated flowfield increased the standard deviation computed from the pressure-time history considerably above the incoming turbulent boundary-layer value (at $\gamma = 3.9\%$, $\sigma_{p_w}/\sigma_{p_{wo}}$ was 2.4).

As the intermittency increased ($\gamma > 25\%$), the shock wave spent more time upstream of the pressure transducer, and enough pressure fluctuations from the separated flowfield were present to visibly skew the actual PDF into a bimodal distribution. The second peak that formed in the actual PDF occurred at a higher pressure level than the peak caused by the incoming turbulent boundary layer and occurred at a pressure level that depended on the JSPR. This trend of the second peak occurring at a higher pressure as the JSPR was increased is consistent with the results found from the streamwise mean pressure distribution measurements made with the static pressure taps along the lower wall of the freestream. Thus, the cause of the second peak in the actual PDF was clearly the pressure fluctuations present in the separated flowfield downstream of the instantaneous shock wave location. In SWBLI studies produced by solid protuberances,[7,8] PDF estimates of the pressure fluctuation amplitudes across the intermittent region were also found to be strongly skewed from equivalent Gaussian distributions and to exhibit the same bimodal nature as found in the current PIBLS experiments.

Higher-Order Moments

The first four moments (mean, variance, skewness, and kurtosis) were computed for each pressure-time history in the upstream and downstream pressure transducer data sets. For each moment, the data from both pressure transducers collapsed on each other over the entire intermittent region when plotted against intermittency.

The mean wall pressure $\bar{p}_w$ is shown in Fig. 6. The mean wall pressure continuously increased over the intermittent region from an incoming turbulent boundary-layer pressure of 29.6 kPa at $\gamma = 0\%$ to an extrapolated pressure of 52.4 kPa at $\gamma = 100\%$. The mean pressure increased in a nonlinear manner over the intermittent region because the pressure level increased in the separated flowfield and the region of separated flow extended farther upstream as the JSPR increased.

The standard deviation of the pressure fluctuations (σ_{p_w}), nondimensionalized by the local mean pressure, is shown in Fig. 7. From a second-order polynomial equation that was least-squares curve fitted to each experimental data set (shown as lines in Fig. 7), $\sigma_{p_w}/\bar{p}_w$ reached a maximum value of 0.22 at $\gamma = 55\%$.

The occurrence of a local maximum in the rms pressure distribution over the intermittent region is a characteristic found in all

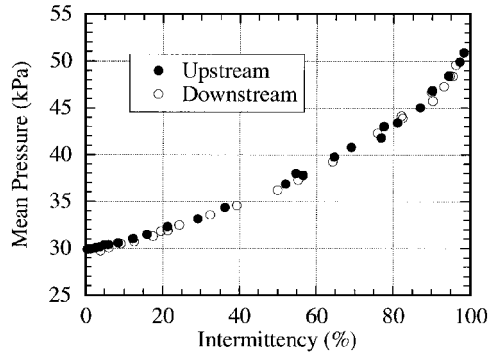

Fig. 6 Mean pressure vs intermittency across the intermittent region of the PIBLS wind tunnel.

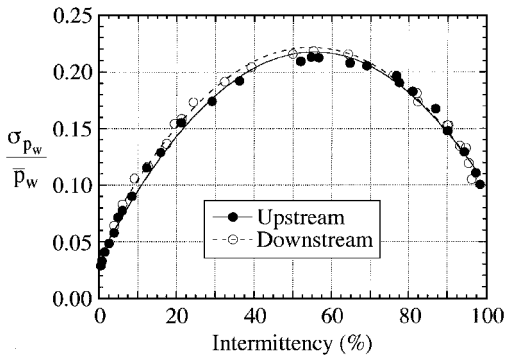

Fig. 7 Nondimensionalized standard deviation of the pressure fluctuations vs intermittency across the intermittent region.

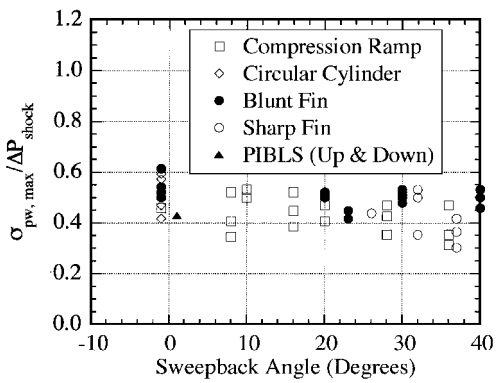

Fig. 8 Strength of the unsteady shock wave motion over the intermittent region for several SWBLI studies.

separated SWBLI flowfields that contain unsteady shock wave motion. For unswept compression ramps at Mach 3, maximum values of $\sigma_{p_w}/\bar{p}_w$ were found to be 0.20 ($\delta_0 = 22$ mm) and 0.18 ($\delta_0 = 12$ mm) for a 24-deg ramp[6] and 0.15 ($\delta_0 = 22$ mm) and 0.11 ($\delta_0 = 22$ mm) for 20- and 16-deg ramps,[7] respectively. The maximum value of $\sigma_{p_w}/\bar{p}_w$ for a 28-deg unswept compression ramp interaction at Mach 5 (Ref. 9) was found to be 0.34. Dolling and Smith[10] reported maximum values of $\sigma_{p_w}/\bar{p}_w$ between 0.25 and 0.28 for circular cylinders at Mach 5, whereas Dolling and Bogdonoff[13] reported values ranging between 0.18 and 0.29 for hemicylindrical blunt fins at Mach 3. Thus, the maximum $\sigma_{p_w}/\bar{p}_w$ value of 0.22 for the PIBLS experiments at Mach 2.5 is within the range of values found in other SWBLI flowfields.

The strength of the unsteady shock wave motion, defined as $\sigma_{p_w,\max}/\Delta P_{\text{shock}}$ (where ΔP_{shock} is the mean static pressure difference across the intermittent region, $\Delta P_{\text{shock}} = \bar{p}_{w,\gamma=96\%} - \bar{p}_{wo}$), for the PIBLS flowfield measurements was calculated to be 0.43. The strengths of the unsteady shock wave motion in compression ramp, circular cylinder, and blunt- and sharp-edged fin interactions[15] are plotted as $\sigma_{p_w,\max}/\Delta P_{\text{shock}}$ vs sweepback angle in Fig. 8, along with the results from the current PIBLS wind-tunnel experiments. In Fig. 8, all of the results for the unswept cases[15] are offset to a sweepback angle of -1 deg, and the results from the PIBLS wind-tunnel experiments are offset to a sweepback angle of $+1$ deg for clarity. The mean value of $\sigma_{p_w,\max}/\Delta P_{\text{shock}}$ for all three solid protuberance geometries and all sweepback angles was 0.46. Thus, the strength of the separation shock wave motion was essentially the same in the PIBLS flowfield as in the SWBLI flowfields produced by solid geometries.

Although not shown here due to length constraints,[20] the skewness coefficient α_3 and kurtosis coefficient α_4 have also been computed for this PIBLS interaction. Both coefficients are noteworthy because of the large maximum values they attain near the line of upstream influence ($\alpha_3 = 5.9$ and $\alpha_4 = 62.8$ at $\gamma = 1.4\%$). A large maximum value of α_3 near the line of upstream influence is a characteristic that has been observed in many SWBLI experiments involving solid protuberances. The maximum value of α_3 near the line of upstream influence ranged between 8 and 10 for circular cylinder interactions[10] at Mach 5, between 7 and 8 for unswept compression ramp interactions[6,7] at Mach 3, and between 6 and 8 for hemicylindrical blunt fin interactions[13] at Mach 3. No maximum values for α_4 have been reported in the literature.

PSD Estimates of the Pressure Fluctuations

For a pressure-time history $p(t)$ in which the time history is divided into n_d contiguous segments and each segment contains N data values ($p_{i,n}$; $n = 0, 1, \ldots, N-1$, and $i = 1, 2, \ldots, n_d$), the one-sided PSD function is estimated by

$$G_{pp}(f_k) = \frac{2}{n_d N \Delta t} \sum_{i=1}^{n_d} |P_i(f_k)|^2, \qquad k = 0, 1, \ldots, N/2 \quad (2)$$

where Δt is the time between consecutive pressure realizations in $p(t)$ and the discrete fast Fourier transform components for each segment are given by

$$P_i(f_k) = \Delta t \sum_{n=0}^{N-1} p_{i,n} \exp\left(\frac{-j2\pi kn}{N}\right) \quad (3)$$

at the discrete frequencies $f_k = k/(N \times \Delta t)$, $k = 0, 1, \ldots, N-1$.

For the purposes of computing the PSD estimates reported herein, each pressure-time history was divided into 488 contiguous segments ($n_d = 488$) having 8192 pressure realizations ($N = 8192$) in each segment. The frequency resolution of the PSD estimates Δf is given by $\Delta f = 1/(N \times \Delta t)$ to be 12.2 Hz, and the normalized random error of the PSD estimates ε_r is given by $\varepsilon_r = 1/\sqrt{n_d}$ to be 4.5%. PSD estimates of the pressure fluctuations computed from the downstream pressure transducer measurements are shown in Fig. 9 for the incoming boundary-layer upstream of the intermittent region, for the intermittent region at five strategic JSPRs, and for the separated flowfield downstream of the intermittent region at a JSPR of 2.55. The PSD estimates shown in Fig. 9 are plotted as $G_{pp}(f) \times f/\sigma^2_{p_w}$ vs f in a linear-log format. Each PSD estimate was normalized by the variance of the pressure-time history. Although this normalization was beneficial for comparison purposes, care must be taken when examining the magnitude of the normalized PSD estimates for the incoming boundary layer and the separated region because the variance of the pressure fluctuations (due to turbulence) in these two flow regimes may be underestimated due to frequency response limitations of the pressure transducers. Remember, however, that it is the pressure fluctuations caused by the much lower frequency separation shock wave motion (at intermediate intermittencies) that are of primary interest here.

The PSD estimate of the pressure fluctuations in the incoming boundary layer was dominated by frequency components below a few hundred hertz. Except for a disturbance centered at 387 Hz (which was found to be caused by the somewhat abrupt geometrical transition between the plenum chamber and the wind-tunnel inlet pipes), these pressure fluctuations were not caused by physical disturbances in the boundary layer but were due to resonance effects associated with the reference port passageway of the pressure transducer. Although the pressure fluctuations caused by resonance in this passageway dominate the PSD estimate in the incoming boundary layer, these pressure fluctuations are small compared with the

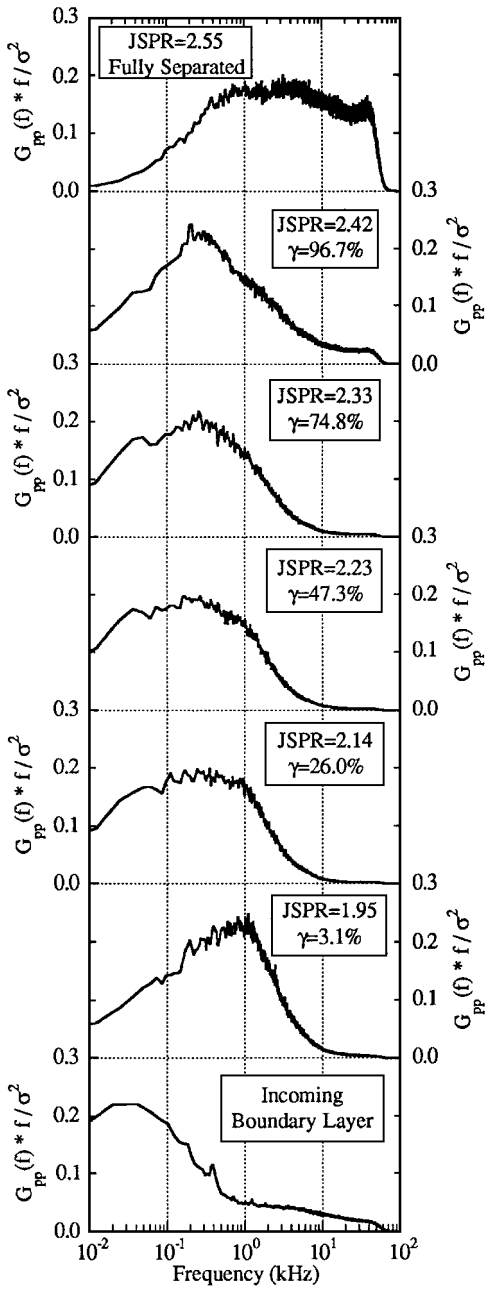

Fig. 9 Normalized power spectral density estimates of the pressure fluctuations across the intermittent region.

pressure fluctuations due to shock wave crossings that appear in the pressure-time histories across the intermittent region, and therefore these pressure fluctuations have no effect on the PSD estimates across the intermittent region.

The PSD estimates computed for the pressure-time histories taken from the intermittent region showed that most of the energy in the pressure fluctuations was concentrated over the frequency range between about 100 Hz and a few thousand hertz. For pressure fluctuations above 10 kHz, the PSD estimates contained no significant energy until the highest intermittencies, e.g., $\gamma = 96.7\%$, were reached. The energy of the pressure fluctuations taken from the fully separated flowfield was distributed uniformly over a frequency range between a few hundred hertz and 50 kHz (the cutoff frequency of the analog filter). This change in the PSD distribution occurred because the PSD estimates taken from the intermittent region were dominated by the large pressure fluctuations caused by the separation shock wave translating over the pressure transducer, whereas the PSD estimate from the fully separated region contains high-frequency pressure fluctuations caused by turbulence in the shear layer and separated region. Thus, the PSD estimates from the intermittent region of the PIBLS flowfield show that the frequency of the shock wave motion was broadband, with most of the energy occurring over a frequency range from approximately 100 Hz to a few thousand hertz, depending on the exact location within the intermittent region.

The energy of the pressure fluctuations acquired from the intermittent region of unswept compression ramp interactions[7,8] was also distributed over the frequency range from a few hundred to a few thousand hertz. Although the PSD estimates for the various ramp angles (16–28 deg) had the same basic broadband shape, the dominant center frequency of the spectral distribution was dependent on the ramp angle. The center frequency decreased as the ramp angle increased. The center frequency was approximately 1000 Hz for a 16-deg ramp angle, 500–1800 Hz for a 20-deg ramp angle, and 200–500 Hz for 24- and 28-deg ramp angles. Thus, the spectral characteristics of the energy in the pressure fluctuations from the intermittent region of the PIBLS flowfield were very similar to the spectral characteristics of the unswept compression ramp interaction at the larger ramp angles of 24 and 28 deg.

Conclusions

The unsteady characteristics of the separation shock wave motion in a plume-induced separated flowfield were determined from pressure measurements made with in situ and remote pressure transducers over the jet static pressure ratio range from 1.95 to 2.55. Time-series analysis techniques were applied to the pressure fluctuation measurements taken from upstream, across, and downstream of the intermittent region. The PDF estimates of the pressure fluctuation amplitudes computed from the intermittent region were highly skewed from the equivalent Gaussian distributions and typically were bimodal in character at intermittencies greater than approximately 25%. The maximum value of $\sigma_{p_w}/\bar{p}_w$ over the intermittent region was found to be 0.22 at $\gamma = 55\%$, and the strength of the unsteady shock wave motion (defined as $\sigma_{p_w,\max}/\Delta P_{\text{shock}}$) for these experiments was calculated to be 0.43. PSD estimates from the intermittent region show that the frequency of the shock wave motion was broadband, with most of the energy occurring over a frequency range from approximately 100 Hz to a few thousand hertz.

In conclusion, many of the statistical properties computed for this plume-induced separated flowfield were qualitatively similar to the statistical properties computed for two-dimensional shock wave/boundary-layer interaction flowfields produced by solid geometries. This is true even though the size of the separated region is much larger for this plume-induced separated flow than for solid boundary-induced separation and although the PIBLS separated region is enclosed by two fluid dynamically compliant shear layers rather than by a solid boundary and a single shear layer. Perhaps these observations will help shed some light on the source of the large-scale unsteadiness mechanisms in shock wave/boundary-layer interactions. In any event, it is clear that the unsteady separation process that can accompany the occurrence of plume-induced, boundary-layer separation in high-speed flight is important because of the large aerodynamic loads that occur over a broad frequency range.

Acknowledgments

This work was sponsored by the U.S. Army Research Office under Grant DAAH04-93-G-0226 and was monitored by Thomas L. Doligalski. This source of support is gratefully acknowledged. Also, the authors would like to thank David S. Dolling for generously providing the conditional analysis algorithm. The authors would like to extend special thanks to Jeff Herrin for his assistance with the laser Doppler velocimeter measurements.

References

[1] Jones, J. H., "Acoustic Environment Characteristics of the Space Shuttle," *Space Transportation System Technology Symposium*, NASA TM-X-52876, Vol. 2—Dynamics and Aeroelasticity, NASA Lewis Research Center, Cleveland, OH, 1970, pp. 285–300.

[2] Boggess, A. L., "An Investigation of the Unsteady Flow Associated with Plume Induced Flow Separation," Bureau of Engineering Research, Univ. of Alabama, Rept. 149-02, Tuscaloosa, AL, 1972.

[3] Doughty, J. O., "Effects of Periodic Plume Pulsing on the Flow Field Generated by Plume Induced Flow Separation," Bureau of Engineering Research, Univ. of Alabama, Rept. 164-02, Tuscaloosa, AL, 1973.

[4]Doughty, J. O., "A Study of a Plume Induced Separation Shock Wave, Including Effects of Periodic Plume Unsteadiness," Bureau of Engineering Research, Univ. of Alabama, Rept. 207-02, Tuscaloosa, AL, 1976.

[5]Dolling, D. S., "Unsteadiness of Shock-Wave Induced Turbulent Boundary-Layer Separation—A Review," *Turbulent Shear-Layer/Shock-Wave Interactions*, edited by J. M. Délery, Springer–Verlag, Berlin, 1986, pp. 341–357.

[6]Dolling, D. S., and Murphy, M. T., "Unsteadiness of the Separation Shock Wave Structure in a Supersonic Compression Ramp Flowfield," *AIAA Journal*, Vol. 21, No. 12, 1983, pp. 1628–1634.

[7]Dolling, D. S., and Or, C. T., "Unsteadiness of the Shock Wave Structure in Attached and Separated Compression Ramp Flows," *Experiments in Fluids*, Vol. 3, No. 1, 1985, pp. 24–32.

[8]Erengil, M. E., and Dolling, D. S., "Effects of Sweepback on Unsteady Separation in Mach 5 Compression Ramp Interactions," *AIAA Journal*, Vol. 31, No. 2, 1993, pp. 302–311.

[9]Gramann, R. A., and Dolling, D. S., "Detection of Turbulent Boundary-Layer Separation Using Fluctuating Wall Pressure Signals," *AIAA Journal*, Vol. 28, No. 6, 1990, pp. 1052–1056.

[10]Dolling, D. S., and Smith, D. R., "Separation Shock Dynamics in Mach 5 Turbulent Interactions Induced by Cylinders," *AIAA Journal*, Vol. 27, No. 12, 1989, pp. 1698–1706.

[11]Gibson, B. T., and Dolling, D. S., "Exploratory Study of Wall Pressure Fluctuations in a Mach 5, Sharp Fin-Induced Turbulent Interaction," *AIAA Journal*, Vol. 30, No. 9, 1992, pp. 2188–2195.

[12]Schmisseur, J. D., and Dolling, D. S., "Fluctuating Wall Pressures near Separation in Highly Swept Turbulent Interactions," *AIAA Journal*, Vol. 32, No. 6, 1994, pp. 1151–1157.

[13]Dolling, D. S., and Bogdonoff, S. M., "An Experimental Investigation of the Unsteady Behavior of Blunt Fin-Induced Shock Wave Turbulent Boundary Layer Interactions," AIAA Paper 81-1287, 1981.

[14]Brusniak, L., and Dolling, D. S., "Flowfield Dynamics in Blunt Fin-Induced Shock Wave Turbulent Boundary-Layer Interaction," AIAA Paper 93-3133, July 1993.

[15]Gonsalez, J. C., and Dolling, D. S., "Correlation of Interaction Sweepback Effects on the Dynamics of Shock-Induced Turbulent Separation," AIAA Paper 93-0776, Jan. 1993.

[16]Erengil, M. E., and Dolling, D. S., "Physical Causes of Separation Shock Unsteadiness in Shock Wave/Turbulent Boundary-Layer Interactions," AIAA Paper 93-3134, July 1993.

[17]Dolling, D. S., "Fluctuating Loads in Shock Wave/Turbulent Boundary Layer Interaction: Tutorial and Update," AIAA Paper 93-0284, Jan. 1993.

[18]Aso, S., Tan, A., and Hayashi, M., "The Structure of Aerodynamic Heating in Three-Dimensional Shock Wave/Turbulent Boundary Layer Interactions Induced by Sharp and Blunt Fins," AIAA Paper 89-1854, June 1989.

[19]Sun, C. C., and Childs, M. E., "A Modified Wall Wake Velocity Profile for Turbulent Compressible Boundary Layers," *Journal of Aircraft*, Vol. 10, No. 6, 1973, pp. 381–383.

[20]Shaw, R. J., "An Experimental Investigation of Unsteady Separation Shock Wave Motion in a Plume-Induced, Separated Flowfield," Ph.D. Dissertation, Dept. of Mechanical and Industrial Engineering, Univ. of Illinois, Urbana, IL, Oct. 1995.

[21]Fernholz, H. H., and Finley, P. J., "A Critical Commentary on Mean Flow Data for Two-Dimensional Compressible Turbulent Boundary Layers," AGARDograph 253, May 1980.

[22]Raman, K. R., "A Study of Surface Pressure Fluctuations in Hypersonic Turbulent Boundary Layers," NASA CR-2386, 1974.

[23]Bendat, J. S., and Piersol, A. G., *Random Data*, 2nd ed., Wiley, New York, 1986, Chaps. 5 and 7.

[24]Brusniak, L., "Evaluation of Conditional Sampling Methods for Analysing Separation Shock Motion," AIAA Paper 88-0091, Jan. 1988.

[25]Dolling, D. S., and Brusniak, L., "Separation Shock Motion in Fin, Cylinder and Compression Ramp-Induced Turbulent Interactions," *AIAA Journal*, Vol. 27, No. 6, 1989, pp. 734–742.

[26]Erengil, M. E., and Dolling, D. S., "Unsteady Wave Structure near Separation in a Mach 5 Compression Ramp Interaction," *AIAA Journal*, Vol. 29, No. 5, 1991, pp. 728–735.

[27]Kazimierski, Z., and Trojnarski, J., "Time-Averaged Pressure of Fluctuating Gas Motion in Small-Diameter Tubes," *AIAA Journal*, Vol. 25, No. 4, 1987, pp. 567–572.

W. Oberkampf
Associate Editor